Fullerene-like (IF) NbxMo1-xS2 nanoparticles

ARTICLE *in* JOURNAL OF THE AMERICAN CHEMICAL SOCIETY · NOVEMBER 2007

Impact Factor: 12.11 · DOI: 10.1021/ja074081b · Source: PubMed

J|A|C|S
ARTICLES
Published on Web 09/21/2007

Fullerene-Like (IF) $Nb_xMo_{1-x}S_2$ Nanoparticles

Francis Leonard Deepak,[†] Hagai Cohen,[‡] Sidney Cohen,[‡] Yishay Feldman,[‡] Ronit Popovitz-Biro,[§] Doron Azulay,[||] Oded Millo,[||] and Reshef Tenne*,[†]

Contribution from the Department of Materials and Interfaces, Chemical Services Unit, Electron Microscopy Unit, Weizmann Institute of Science, Rehovot 76100, Israel, and Racah Institute of Physics, The Hebrew University of Jerusalem, Jerusalem 91904, Israel

Received June 5, 2007; E-mail: reshef.tenne@weizmann.ac.il

Abstract: IF-$Mo_{1-x}Nb_xS_2$ nanoparticles have been synthesized by a vapor-phase reaction involving the respective metal halides with H_2S. The IF-$Mo_{1-x}Nb_xS_2$ nanoparticles, containing up to 25% Nb, were characterized by a variety of experimental techniques. Analysis of the powder X-ray powder diffraction, X-ray photoelectron spectroscopy, and different electron microscopy techniques shows that the majority of the Nb atoms are organized as nanosheets of NbS_2 within the MoS_2 host lattice. Most of the remaining Nb atoms (3%) are interspersed individually and randomly in the MoS_2 host lattice. Very few Nb atoms, if any, are intercalated between the MoS_2 layers. A sub-nanometer film of niobium oxide seems to encoat the majority of the nanoparticles. X-ray photoelectron spectroscopy in the chemically resolved electrical measurement mode (CREM) and scanning probe microscopy measurements of individual nanoparticles show that the mixed IF nanoparticles are metallic independent of the substitution pattern of the Nb atoms in the lattice of MoS_2 (whereas unsubstituted IF-MoS_2 nanoparticles are semiconducting). Furthermore the IF-$Mo_{1-x}Nb_xS_2$ nanoparticles are found to exhibit interesting single electron tunneling effects at low temperatures.

1. Introduction

MoS_2 and WS_2 are quasi two-dimensional (2D) compounds. Atoms within a layer are bound by strong covalent forces, while individual layers are held together by van der Waals (vdW) interactions. The stacking sequence of the layers can lead to the formation of a hexagonal polymorph with two layers in the unit cell (2H), rhombohedral with three layers (3R), or trigonal with one layer (1T). The weak interlayer vdW interactions offer the possibility of introducing foreign atoms or molecules between the layers via intercalation. Furthermore, MoS_2, WS_2, and a plethora of other 2D compounds are known to form closed cage structures which are referred to as inorganic fullerene-like (IF) and inorganic nanotubes (INT), analogous to structures formed from carbon.[1−4] One of the initial methods of synthesis of IF-MoS_2 and IF-WS_2 involved starting from the respective oxide nanoparticles.[5−7] Subsequently synthesis using a gas-phase reaction starting from $MoCl_5$ and H_2S has been demonstrated.[8a] A similar strategy for the synthesis of IF-MoS_2 nanoparticles using the gas-phase reaction between $Mo(CO)_6$ and sulfur has been reported.[8b] The two kinds of reactions progress along very different paths, which has a large effect on the topology of the closed-cage nanoparticles. The conversion of the metal-oxide nanoparticles to sulfides (IF) starts on the surface of the nanoparticles progressing gradually inward in a slow diffusion-controlled fashion. Contrarily, the gas-phase reaction proceeds by a nucleation and growth mode starting from, e.g., a small MoS_2 nuclei and progressing outward rather rapidly.

Following the successful synthesis of the IF nanoparticles and nanotubes, foreign atoms have been incorporated into their lattice by intercalation of IF nanoparticles and by doping/alloying in the case of inorganic nanotubes. For instance IF nanoparticles of MoS_2 and WS_2 were intercalated by exposure to alkali metal (potassium and sodium) vapor using a two-zone transport method.[9a] The intercalation in these compounds is mediated by their structure and can bring about significant changes in their structure and their physical properties. By

[†] Department of Materials and Interfaces, Weizmann Institute of Science.
[‡] Department of Chemical Research Support, Weizmann Institute of Science.
[§] Electron Microscopy Unit, Weizmann Institute of Science.
[||] The Hebrew University of Jerusalem.

(1) Tenne, R. *Nat. Nanotechnol.* **2006**, *1*, 103.
(2) Tenne, R. *J. Mater. Res.* **2006**, *21*, 2726.
(3) Satyanarayana Kuchibhatla, V. N. T.; Karakoti, A. S.; Debasis, Bera.; Seal, S. *Prog. Mater. Sci.* **2007**, *52*, 699.
(4) Remskar, M. *Adv. Mater.* **2004**, *16*, 1497.
(5) Tenne, R.; Margulis, L.; Genut, M.; Hodes, G. *Nature* **1992**, *360*, 444.
(6) Margulis, L.; Salitra, G.; Tenne, R.; Talianker, M. *Nature* **1993**, *365*, 113.
(7) Feldman, Y.; Wasserman, E.; Srolovitz, D. J.; Tenne, R. *Science* **1995**, *267*, 222.
(8) (a) Deepak, F. L.; Margolin, A.; Wiesel, I.; Bar-Sadan, M.; Popovitz-Biro, R.; Tenne, R. *NANO* **2006**, *1*, 167. (b) Etzkorn, J.; Therese, H. A.; Rocker, F.; Zink, N.; Kolb, Ute.; Tremel, W. *Adv. Mater.* **2005**, *17*, 2372.
(9) (a) Zak, A.; Feldman, Y.; Lyakhovitskaya, V.; Leitus, G.; Popovitz-Biro, R.; Wachtel, E.; Cohen, H.; Reich, S.; Tenne, R. *J. Am. Chem. Soc.* **2002**, *124*, 4747. (b) Friend, R. H.; Yoffe, A. D. *Adv. Phys.* **1987**, *36*, 1. (c) Levy, F. *Intercalated Layered Materials*; Reidel Publishing Company: Holland, 1979; Vol. 6. (d) Jaglicic, Z.; Jeromen, A.; Trontelj, Z.; Mihailovic, D.; Arcon, D.; Remskar, M.; Mrzel, A.; Dominko, R.; Gaberscek, M.; Martinez-Agudo, J. M.; Gómez-Garcia, C .J.; Coronado, E. *Polyhedron* **2003**, *22*, 2293. (e) Arcon, D.; Zorko, A.; Cevec, P.; Mrzel, A.; Remskar, M.; Dominko, R.; Gaberscek, M.; Mihailovic, D. *Phys. Rev. B* **2003**, *67*, 125423. (f) Mihailovic, D.; Jaglicic, Z.; Arcon, D.; Mrzel, A.; Zorko, A.; Remskar, M.; Kabanov, V. V.; Dominko, R.; Gaberscek, M.; Go'mez-Garcia, C .J.; Martinez-Agudo, J. M.; Coronado, E. *Phys. Rev. Lett.* **2003**, *90*, 146401−1. (g) Krusin-Elbaum, L.; Newns, D. M.; Zeng, H.; Derycke, V.; Sun, J. Z.; Sandstrom, R. *Nature* **2004**, *431*, 672. (h) Tenne, R. *The Chemistry of Nanostructured Materials*; World Scientific: Singapore, 2003.

variation of the intercalant and its concentration, a large number of compounds with different properties can be prepared.[9b,c] Intercalation is also known in inorganic nanotubes for instance in the case of the Li-intercalation of MoS_2[9d−f] and VO_x nanotubes.[9g] Intercalated compounds are of interest for their electrochemical applications such as solid electrolytes, solid cathodes, batteries, and others such as superconductivity, spintronics, and catalysis.[9h]

Alloying (doping) of inorganic nanotubes has been also reported for specific cases of Ti-doped MoS_2 nanotubes, Nb-doped WS_2 nanotubes, and Mo- and C-doped WS_2 nanotubes.[10a−d] W-alloyed MoS_2 nanotubes have been synthesized by varying the W/Mo ratio.[10e−g] The effect of Nb substitution on the electronic structure of MoS_2 was investigated theoretically using the density functional tight binding method (DFTB).[11] These works predict that mixed $Mo_{1-x}Nb_xS_2$ nanotubes (with varying Nb contents) should exhibit metallic character, independent of their chirality, diameters, and ordering type of the substitutional atoms. In effect the density of states close to the Fermi level of the Nb-substituted MoS_2 tubes can be tuned over a wide range by the degree of Nb doping. Until now, these electronic modifications by dopants have not been experimentally verified either in IF nanoparticles or in nanotubes.

The structure of MoS_2 and NbS_2 can be described as follows. In analogy with graphite, the unit cell of MoS_2 is made of two layers in hexagonal arrangement (2H). The Mo atom is covalently bonded to six sulfur atoms in trigonal biprism coordination. The interlayer spacing ($c/2$) is 6.15 Å. The interlayer spacing in the case of the IF-MoS_2 nanoparticles (6.2 Å) is slightly larger than the $c/2$ parameter of bulk 2H-MoS_2 polytype (6.15 Å).[1,2,5−7] This expansion seen in the case of the IF-MoS_2 nanoparticles serves to alleviate the strain involved in the folding of the IF structure. In the case of NbS_2, the various Nb−S phases were first investigated by Jellinek et al.[12a,b] Two polymorphs of the layered disulfide were identified: the rhombohedral-3R ($R3m$) polytype with a unit cell consisting of three NbS_2 slabs which is formed when the elements are heated below 800 °C. In this case the interlayer spacing was found to be 5.96 Å. The hexagonal-2H ($P63/mmc$) polymorph with a unit cell consisting of two NbS_2 slabs is obtained above 850 °C. The $c/2$ spacing is 5.981 Å in this case. In both polytypes the Nb is bonded to six neighboring sulfur atoms in octahedral coordination. Nonstoichiometric 3R-$Nb_{1+x}S_2$ compounds were also found.[12b] Further studies showed that the 3R polytype exists in the range $0 < x < 0.18$, while the 2H polytype is stable only for small deviations from stoichiometry.[12c] Both phases exhibit metallic behavior, and the 2H-phase shows even superconductivity below 6.23 K.[12c] It was noticed that the excess niobium atoms are actually intercalated in the vdW gap between each of the two NbS_2 layers. In the case of the IF-NbS_2 nanoparticles, which were synthesized by gas-phase reaction, the interlayer spacing was found to be in the range 5.9−6.35 Å for the small (20−40 nm) particles and 6.2 Å for the larger (60−80 nm) ones. Annealing the as-obtained IF-NbS_2 nanoparticles resulted in a layer spacing varying from 6.15 to 5.9 Å and more faceted nanoparticles.[12d] Mixed bulk crystals of MoS_2/NbS_2 were prepared by heating the respective elements for days in the presence of small amounts of iodine as well as by chemical vapor transport.[12e]

In the current study mixed phase IF-$Mo_{1-x}Nb_xS_2$ nanoparticles were prepared by a vapor-based method starting from the respective volatile metal chloride precursors in combination with H_2S. This method has been previously used for the successful synthesis of IF-MoS_2 nanoparticles and nanotubes.[8a] The use of metal chloride precursors to obtain IF-NbS_2, IF-TaS_2, and IF-TiS_2 nanoparticles by the vapor-phase reaction, albeit by different means is well established.[12d,13,14] One of the main advantages of this method is that, being a vapor-phase synthesis, it allows intimate mixing of the materials, namely Nb, in this case with that of Mo. The IF-$Mo_{1-x}Nb_xS_2$ nanoparticles have been characterized and extensively studied. It has been found that, for $Mo_{1-x}Nb_xS_2$ with values of $x \leq 0.3$, the 2H modification is formed. Bulk $Mo_{1-x}Nb_xS_2$ particles of the mixed phases with a higher content of niobium however crystallize like NbS_2 in the 3R modification.[12e] Interestingly, the IF-$Mo_{1-x}Nb_xS_2$ nanoparticles exhibited metallic behavior, consistent with recent theoretical calculations. This is a remarkable demonstration that doping can significantly affect the electronic properties of semiconducting IF nanoparticles and, in particular, drive a semiconductor to metal transition.

2. Experimental Section

The synthesis of the IF-$Mo_{1-x}Nb_xS_2$ nanoparticles was carried out starting from the precursors $MoCl_5$ (purchased from Aldrich) and $NbCl_5$ (purchased from Alfa Aesar) in reaction with H_2S using the vertical reactor[8a,14] by a two-stage furnace setup (Figure 1). Before each growth session, the vertical reactor (Figure 1a) (which was preset to higher temperatures of about 600 °C) was purged continuously with N_2 in order to prevent traces of O_2 and water vapor that would otherwise interfere with the course of the reaction. The precursors 0.550 g of $MoCl_5$ (mp = 194 °C, bp = 268 °C) and 0.010 g of $NbCl_5$ (mp = 204.7 °C, bp = 254 °C) were first heated in the auxiliary furnace to a temperature of ∼250 °C (T_4) (Figure 1b). In order to avoid condensation of the vapors of the precursor, before it reaches the vertical reactor, a preset temperature of 220 °C (T_3) was maintained along the length of the tube connecting the auxiliary and main reactors (see experimental setup, Figure 1) using a heating band. The vapors of the precursor were carried from below into the hot zone (kept at a preset temperature) by flowing 50 cm^3 of forming gas (I) (95% N_2 and 5% H_2). Forming gas was used to ensure complete reduction of the metal chloride precursors. Simultaneously, 5 cm^3 of H_2S (II) was introduced from above mixed along with 50 cm^3 of N_2 (III). The typical time period for each reaction was 30 min. Two series of reactions (Table 1) were carried out wherein the temperature of the main vertical furnace (Figure 1a) was maintained at (i) T_1 = 800 °C and T_2 = 850 °C (series 1) and (ii) T_1 = 850 °C and

(10) (a) Zhu, Y. Q.; Hsu, W. K.; Terrones, M.; Firth, S.; Grobert, N.; Clark, R. J. H.; Kroto H. W.; Walton, D. R. M. *Chem. Commun.* **2001**, 121. (b) Zhu, Y. Q.; Hsu, W. K.; Terrones, M.; Firth, S.; Grobert, N.; Clark, R. J. H.; Kroto, H. W.; Walton, D. R. M. *Chem. Phys. Lett.* **2001**, *342*, 15. (c) Hsu, W. K.; Zhu, Y. Q.; Yao, N.; Firth, S.; Clark, R. J. H.; Kroto, H. W.; Walton, D. R. M. *Adv. Funct. Mater.* **2001**, *11*, 69. (d) Hsu, W. K.; Zhu, Y. Q.; Bothroyd, C. B.; Kinloch, I.; Trasobares, S.; Terrones, H.; Grobert, N.; Terrones, M.; Escudero, R.; Chen, G. Z.; Colliex, C.; Windle, A. H.; Fray, D. H.; Kroto, H. W.; Walton, D. R. M. *Chem. Mater.* **2000**, *12*, 3541. (e) Nath, M.; Mukhopadhyay, K.; Rao, C. N. R. *Chem. Phys. Lett.* **2002**, *352*, 163. (f) Rao, C. N. R.; Nath, M. *Dalton Trans.* **2004**, 1. (g) Tenne, R.; Rao, C. N. R. *Philos. Trans. R. Soc. London, Ser. A* **2004**, *362*, 2099.
(11) (a) Ivanovskaya, V. V.; Heine, T.; Gemming, S.; Seifert, G. *Phys. Status Solidi B* **2006**, *243*, 1757. (b) Ivanovskaya, V. V.; Seifert, G.; Ivanovskii, A. L. *Russ. J. Inorg. Chem.* **2006**, *51*, 320.
(12) (a) Jellinek, F.; Brauer, G.; Müller, H. *Nature*, **1960**, *185*, 376. (b) Kadijk, F.; Jellinek, F. *J. Less-Common Met.* **1969**, *19*, 421. (c) Fisher, W. G.; Sienko, M. J. *Inorg. Chem.*, **1980**, *19*, 39. (d) Schuffenhauer, C.; Popovitz-Biro, R.; Tenne, R. *J. Mater. Chem.* **2002**, *12*, 1587. (e) Hotje, U.; Binnewies, M. *Z. Anorg. Allg. Chem.* **2005**, *631*, 2467.
(13) Schuffenhauer, C.; Parkinson, B. A.; Jin-Phillipp, N. Y.; Joly-Pottuz, L.; Martin, J.-M.; Popovitz-Biro, R.; Tenne, R. *Small* **2005**, *1*, 1100.
(14) Margolin, A.; Popovitz-Biro, R.; Albu-Yaron, A.; Rapoport, L.; Tenne, R. *Chem. Phys. Lett.* **2005**, *411*, 162.

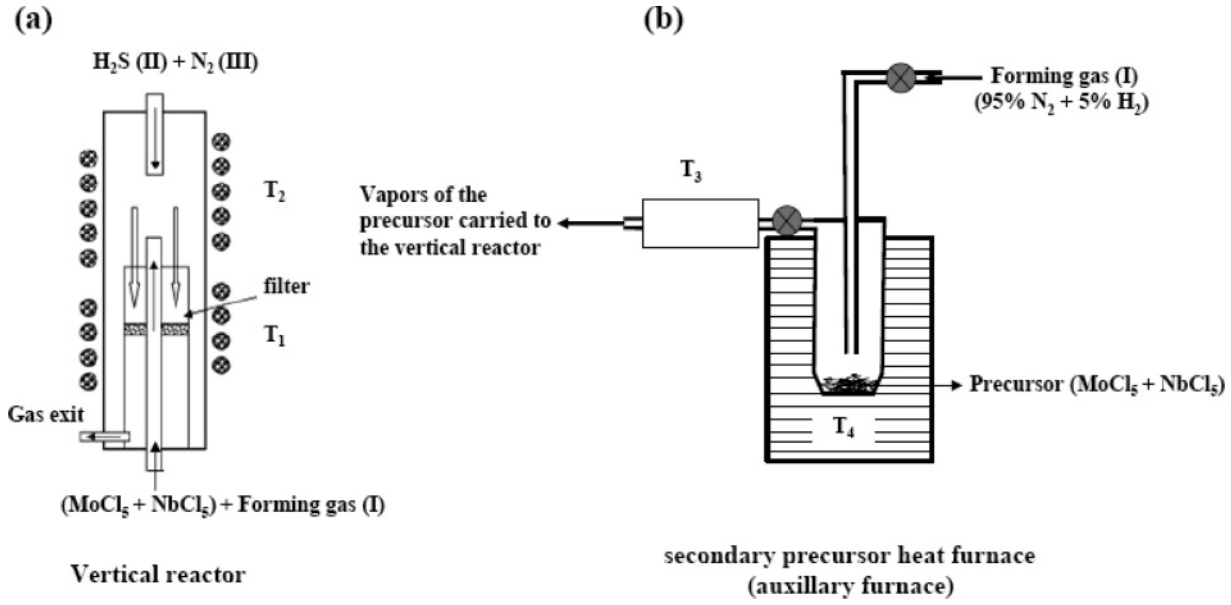

Figure 1. Two-stage furnace setup employed for the synthesis of the IF-$Mo_{1-x}Nb_xS_2$ nanoparticles. (a) Vertical reactor and (b) the secondary precursor heat furnace (auxiliary furnace).

Table 1. Details of the Reactions Carried out for the Synthesis of the IF-$Mo_{1-x}Nb_xS_2$ nanoparticles

temperature of the vertical reactor	temperature of the auxiliary furnace	gas flow rates	size of the IF–$Mo_{1-x}Nb_xS_2$ nanoparticles	description of the as-obtained IF–$Mo_{1-x}Nb_xS_2$ nanoparticles
series 1		forming gas (I) = 50 cm^3 (95% N_2 and 5% H_2)	~50 nm	spherical IF nanoparticles
T_1 = 800 °C	T_3 = 220 °C	H_2S (II) = 5 cm^3		
T_2 = 850 °C	T_4 = 250 °C	N_2 (III) = 50 cm^3		
series 2		forming gas (I) = 50 cm^3 (95% N_2 and 5% H_2)	~40 nm	IF nanoparticles more faceted
T_1 = 850 °C	T_3 = 220 °C	H_2S (II) = 5 cm^3		
T_2 = 900 °C	T_4 = 250 °C	N_2 (III) = 50 cm^3		

T_2 = 900 °C (series 2). At the end of the reaction, the product was collected (as a black colored powder) at the hot zone of the main furnace by means of a quartz wool filter. It was subsequently analyzed by various characterization techniques including X-ray diffraction (XRD); transmission electron microscopy (TEM) coupled with an energy dispersive X-ray analyzer (EDS); high-resolution transmission electron microscopy (HRTEM) equipped with electron energy loss spectroscopy (EELS); X-ray photoelectron spectroscopy (XPS); atomic force microscopy (AFM) and scanning tunneling microscopy (STM); and spectroscopy (STS).

A vertical theta−theta diffractometer (TTRAX III, Rigaku, Japan) equipped with a rotating Cu anode operating at 50 kV and 240 mA was used for X-ray powder diffraction (XRD) studies. The measurements were carried out in the reflection Bragg−Brentano mode within the range of 10°−70° of 2Θ angles. XRD patterns were collected by a scintillation detector. The minute quantities of material available dictated a very slow data rate (0.05°/min). The peak positions and shapes of the Bragg reflections were determined by a self-consistent profile-fitting procedure using the Jade 8 software. XRD was carried out on both the IF-$Mo_{1-x}Nb_xS_2$ (from this work) and IF-MoS_2 nanoparticles (used as a reference).

The following electron microscopes were used in this work: transmission electron microscope (Philips CM120 TEM) operating at 120 kV, equipped with an EDS detector (EDAX-Phoenix Microanalyzer); HRTEM with a field emission gun (FEI Technai F30-UT) operating at 300 kV, equipped with a parallel electron energy loss spectrometer [Gatan imaging filter-GIF (Gatan)]. For electron microscopy and analysis the collected powder was sonicated in ethanol and placed on a carbon-coated Cu grid (for TEM) or on lacy carbon-coated Cu grids (for HRTEM and EELS). The energy windows for the elemental mapping by energy-filtered TEM (EFTEM) were chosen as follows (standard parameters of the software): The sulfur map was measured around the S $L_{2,3}$ edge (167−187 eV); the niobium map was measured around the Nb L_3 edge (2370−2470 eV); the oxygen map was measured around the O K edge (532−562 eV). Elemental maps were obtained with the three window method. Nb mapping required long recording times (50 s for each energy window), while for the other elements a 1−5 s recording time was used.

X-ray photoelectron spectroscopy (XPS) was carried out using a Kratos AXIS-HS spectrometer at a low power (75 W) of the monochromatized Al (Kα) source. Samples were prepared for XPS analyses by depositing a few drops of the nanoparticles, sonicated in ethanol, onto a gold substrate (SPI supplies, thickness 150 nm). An electron flood gun (eFG) was used for varying the surface charging conditions, where its electron kinetic energy ranged between 2 and 4.5 eV.[15a] The eFG was controlled via filament current, and two bias voltages, its beam diameter on a scale of a few millimeters, were subjected to variations upon changes in bias values. Line shifts (e.g., upon switching on the eFG) were determined in a numerical procedure.[15b]

Conducting atomic force microscope (c-AFM) measurements were made on a P47 Solver AFM (NT-MDT, Moscow), using n-doped diamond tips (DCP20, NT-MDT). These probes have a resonance frequency of 500 kHz and a force constant of 70 N/m, with a tip radius

(15) (a) Cohen, H. *Appl. Phys. Lett.* **2004**, *85*, 1271. (b) Doron-Mor, I.; Hatzor, A.; Vaskevich, A.; van der Boom-Moav, T.; Shanzer, A.; Rubinstein, I.; Cohen, H. *Nature* **2000**, *406*, 382.

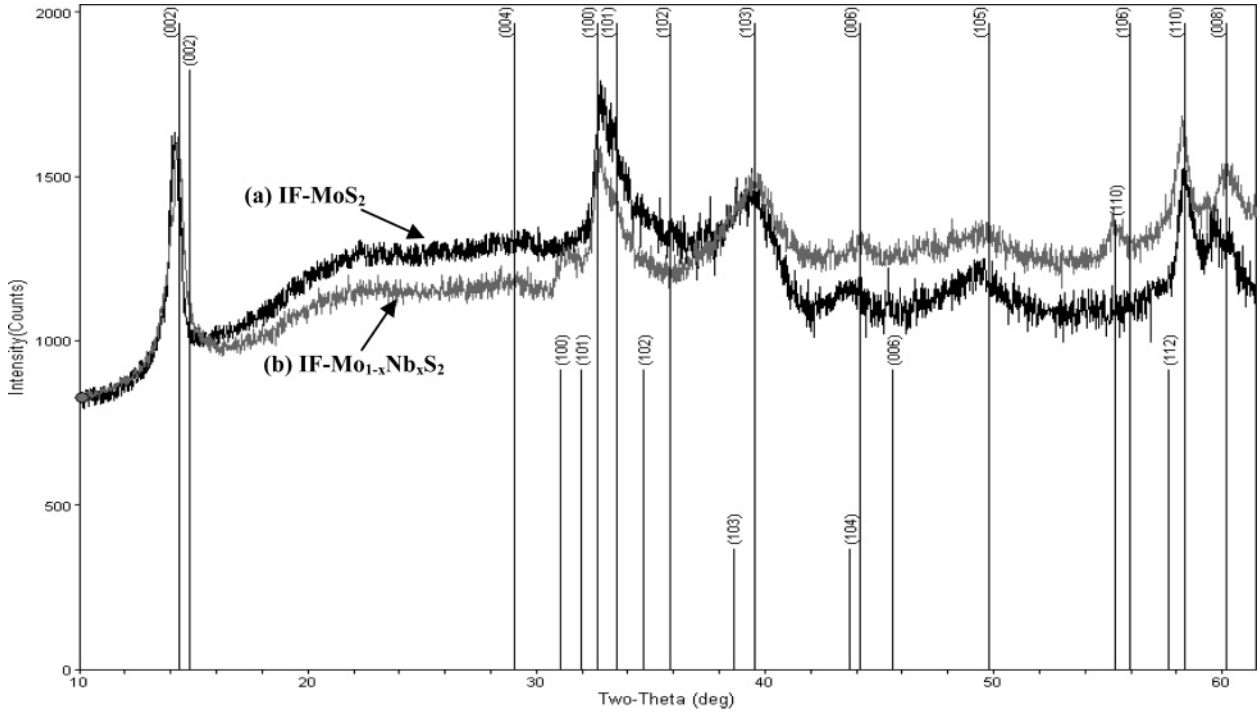

Figure 2. XRD pattern of (a) IF-MoS_2 and (b) nanoparticles prepared at $T_1 = 850$ °C and $T_2 = 900$ °C (series 2). Standard diffraction patterns of 2H-MoS_2 (long lines) and 2H-NbS_2 (short lines) are also shown for comparison.

of 70 nm and rated conductivity of the CVD diamond-like coating of 0.5−1 ohm/cm. Sample topography was recorded in semicontact mode. The AU006 conducting tip holder has an rms noise < 20 pA and gives linear response up to about 10 nA, saturating at 20 nA. Current voltage characteristics (*I*/*V* curves) were measured by placing the tip on the nanoparticle with a small, preset force — 100 nN or less — and sweeping the bias voltage relative to the tip, while collecting current through the tip. *I*/*V* curves measured on clean gold surfaces showed Ohmic behavior, with a resistance of <10 megaohm. At least 10 repeat measurements were made on each of several different nanoparticles of each type, both IF-$Mo_{1-x}Nb_xS_2$ and IF-MoS_2 (used as the reference), to provide suitable statistics. Samples for the AFM measurements were prepared by adding a drop of the nanoparticles sonicated in ethanol onto an atomically flat Au substrate (SPI supplies, thickness 150 nm) or onto Au polycrystalline films coating Si substrates by DC sputtering.

Scanning tunneling microscopy (STM) and spectroscopy (STS) were performed in order to characterize the tunneling-transport properties and density of states of the IF-$Mo_{1-x}Nb_xS_2$ nanoparticles, in comparison with their IF-MoS_2 counterparts. The measurements were performed both at room temperature (in vacuum) and at 4.2 K (in He exchange gas environment, introduced to the STM sample space after evacuation). The samples were prepared as described above for the c-AFM measurements and introduced into a homemade cryogenic STM after being exposed to ambient air for less than 15 min. The tunneling spectra (d*I*/d*V* vs *V* characteristics, proportional to the electronic density of states) were acquired by positioning and stabilizing the STM tip over a specific particle, thus forming a double barrier tunnel junction.[16,17] The STM measurements were performed with the bias applied to the sample and current collected through the tip. About five curves were acquired sequentially at each position to ensure data reproducibility. The spectra were taken with the STM tip retracted as far as possible from the IF nanoparticle in order to minimize the effect of voltage division between the two tunnel junctions, which acts to increase the apparent (measured) gaps.[16]

(16) Banin, U.; Millo, O. *Ann. Rev. Phys. Chem.* **2003**, *54*, 465.
(17) Hanna, A. E.; Tinkham, M. *Phys. Rev. B* **1991**, *44*, R5919.

3. Results and Discussion

3.1. X-ray Diffraction (XRD). Figure 2 shows the XRD pattern obtained from the IF-$Mo_{1-x}Nb_xS_2$ nanoparticles (series 2) synthesized as described above (see Experimental Section). A halo around 22° is due to the traces of amorphous quartz wool, which was used as a filter for collecting the synthesized nanoparticles. From the figure it is seen that the peaks of the first pattern (Figure 2, curve a) match those of IF-MoS_2 nanoparticles (used as a reference), while the second pattern corresponds to that for IF-$Mo_{1-x}Nb_xS_2$ nanoparticles (Figure 2, curve b). The peaks in the IF-$Mo_{1-x}Nb_xS_2$ phase match well with that of IF-MoS_2. A detailed comparison between IF-MoS_2 and IF-$Mo_{1-x}Nb_xS_2$ (Figures 2 and 3) diffraction patterns shows some shifts of the (002) and (110) peaks. Comparing the (002) peaks at ∼14° for both IF-MoS_2 and IF-$Mo_{1-x}Nb_xS_2$ (Figures 2 and 3) one can conclude that one of them (IF-MoS_2, Figure 2, curve a and Figure 3, curve a) has a symmetric shape while the other (IF-$Mo_{1-x}Nb_xS_2$ Figure 2, curve b and Figure 3, curve b) does not. The peak profile (∼14°, Figure 3, curve b) is certainly not symmetric and probably consists of two peaks corresponding to *c*-axis spacings of 6.4 Å and 6.165 Å. The (110) peak at ∼58° of the IF-$Mo_{1-x}Nb_xS_2$ (Figure 2) has a very small shift (about 0.08°) to lower angles with respect to the IF-MoS_2 (110) peak. There are additional peaks at 2.88 Å (31°) and 1.66 Å (55.3°) which are best suited to the (100) and (110) reflections of the 2H-NbS_2 phase. Moreover, the peak profile around 31° exhibits an asymmetry (fast intensity increase and slow decrease with increasing angle) which is similar to the shape of the (100) reflection of IF-MoS_2 at 32.7° (see Figure 2, curve a). This latter peak is a typical example for the strongly asymmetric line shapes of the (*h*00) peaks of layered materials

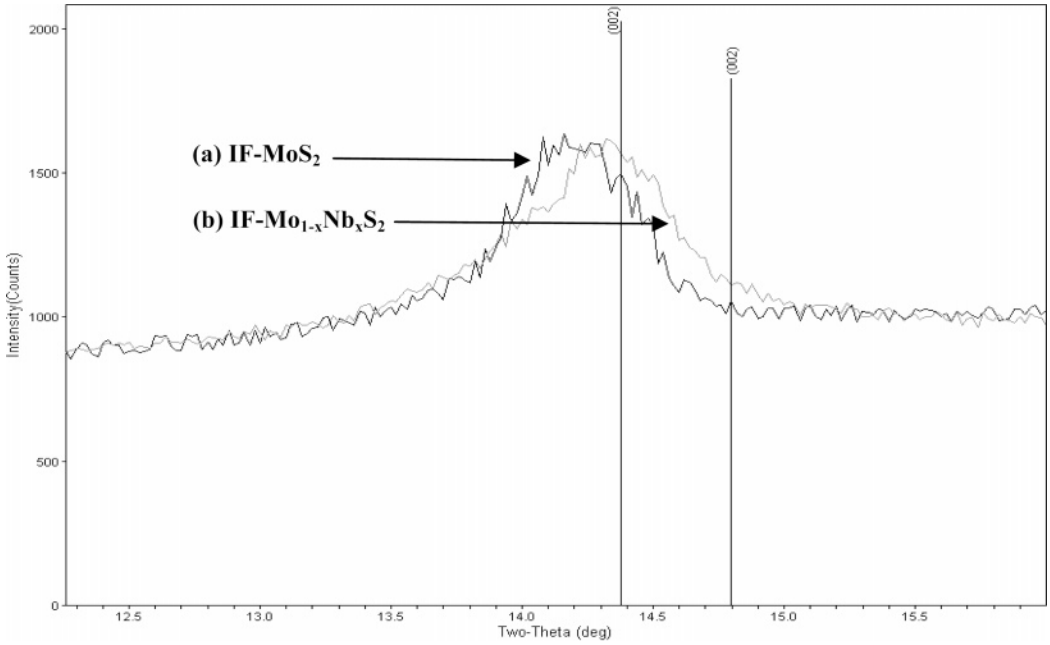

Figure 3. A zoom-in look of (002) peaks from Figure 2. Standard diffraction patterns of 2H-MoS_2 (long line) and 2H-NbS_2 (short line) are also shown for comparison.

with a relatively small number of stacked molecular layers.[18a] The absence of any other NbS_2 peak could be attributed to their relatively small concentration and their poor lattice order, which leads to the low intensity of the NbS_2-related peaks in the noisy spectrum. All the other mixed (*hkl*) peaks would be expected to be suppressed completely if it is assumed that the NbS_2 structures form a turbostratically (misaligned layers) stacked system with randomness in translation and rotation of the layers.[18b] This may also be the reason for the broadening of the (002) peak (~14°) in the case of the IF-$Mo_{1-x}Nb_xS_2$ nanoparticles. Thus the XRD data of the IF-$Mo_{1-x}Nb_xS_2$ nanoparticles suggest the presence of two separate phases within many if not all of the nanoparticles, corresponding to that of Nb-doped MoS_2 and NbS_2 lattices.

3.2. Transmission Electron Microscopy (TEM), Energy Dispersive X-ray Analysis (EDS), and Electron Energy Loss Spectroscopy (EELS). Extensive TEM investigations were carried out on the IF-$Mo_{1-x}Nb_xS_2$ nanoparticles. The TEM and HRTEM images of the IF-$Mo_{1-x}Nb_xS_2$ nanoparticles are shown in Figure 4. Figure 4a shows a collection of IF-$Mo_{1-x}Nb_xS_2$ nanoparticles synthesized at $T_1 = 800$ °C and $T_2 = 850$ °C (series 1). As can be seen from the TEM image, the as-obtained IF nanoparticles are of uniform size distribution (diameter ~50 nm). Figure 4b and 4c present the HRTEM images of the IF-$Mo_{1-x}Nb_xS_2$ nanoparticles prepared at $T_1 = 850$ °C and $T_2 = 900$ °C (series 2), respectively. The diameter of the IF-$Mo_{1-x}Nb_xS_2$ nanoparticles obtained by this reaction is about ~40 nm. However, occasionally some very large IF nanoparticles of about 200 nm in diameter can be also observed. Figure 4d shows the TEM-EDS analysis of the IF-$Mo_{1-x}Nb_xS_2$ nanoparticle shown in Figure 4c. Niobium atoms seem to be uniformly distributed in all the examined nanoparticles, irrespective of their size or shape. The presence of the characteristic and distinct Mo (K,L), S (K), and Nb (K,L) lines can be seen clearly. In comparison to the previous case (series 1), the IF nanoparticles obtained by this reaction (series 2) are much more faceted and well crystallized. This is due to the higher synthesis temperature used in this case. The development of an IF structure displaying improved crystallinity and increased faceting with rising temperature was studied previously in the case of IF-NbS_2 and IF-TaS_2.[12d,13] The IF nanoparticle seen in Figure 4b is reminiscent of a nanotube (nanotubes of undoped MoS_2 were obtained previously in the same temperature regime).[8a] The factors influencing the size of the nanoparticles were discussed in the past, but they are still not fully understood.[8a,12d,13] The growth of the nanoparticles is very fast (<1 s). The supply of the precursor gases is unlimited, and the nanoparticles remain in the hot zone of the reactor until the reaction is turned down (30 min). These observations suggest that the nanoparticles cease to grow due to energetic consideration. Similar considerations were found to control the size of WS_2 (MoS_2) nanotubes.[19]

Shown in Figure 5a and 5b are the HRTEM images and the corresponding EELS spectra of an individual IF-$Mo_{1-x}Nb_xS_2$ nanoparticle prepared at $T_1 = 850$ °C and $T_2 = 900$ °C (series 2). Here again it is seen that the particle is well faceted with clear and sharp curvatures forming the closed-cage nanoparticle (diameter = ~40 nm, no. of layers ~30). The EELS spectrum in Figure 5b showed a good signal-to-noise ratio and very distinct Mo ($L_{3,2}$), S (K), and Nb ($L_{3,2}$) peaks. The Mo/Nb ratio was determined by the integration of the Nb-$L_{3,2}$ edge relative to the Mo-$L_{3,2}$ edge, after background subtraction. This gives an atomic ratio of Nb to Mo of about 0.30:1.00. The metal to sulfur ratio is 1:2. Thus the stoichiometry of the IF-$Mo_{1-x}Nb_xS_2$ nanoparticles is as following: Mo/Nb/S 0.75(±0.05):0.25-(±0.05):2. In order to ascertain whether Nb was present as an intercalant, between the MoS_2 walls, or in substitutional sites in the layers of the MoS_2 lattice, additional TEM-EDS and HRTEM-EELS analyses were performed. The results show that

(18) (a) Yang, D.; Frindt, R. F. *Mol. Liq. Cryst.* **1994**, *244*, 355. (b) Warren, B. E. *Phys. Rev.* **1941**, *59*, 693.

(19) Seifert, G.; Köhller, T.; Tenne, R. *J. Phys. Chem. B* **2002**, *106*, 2497.

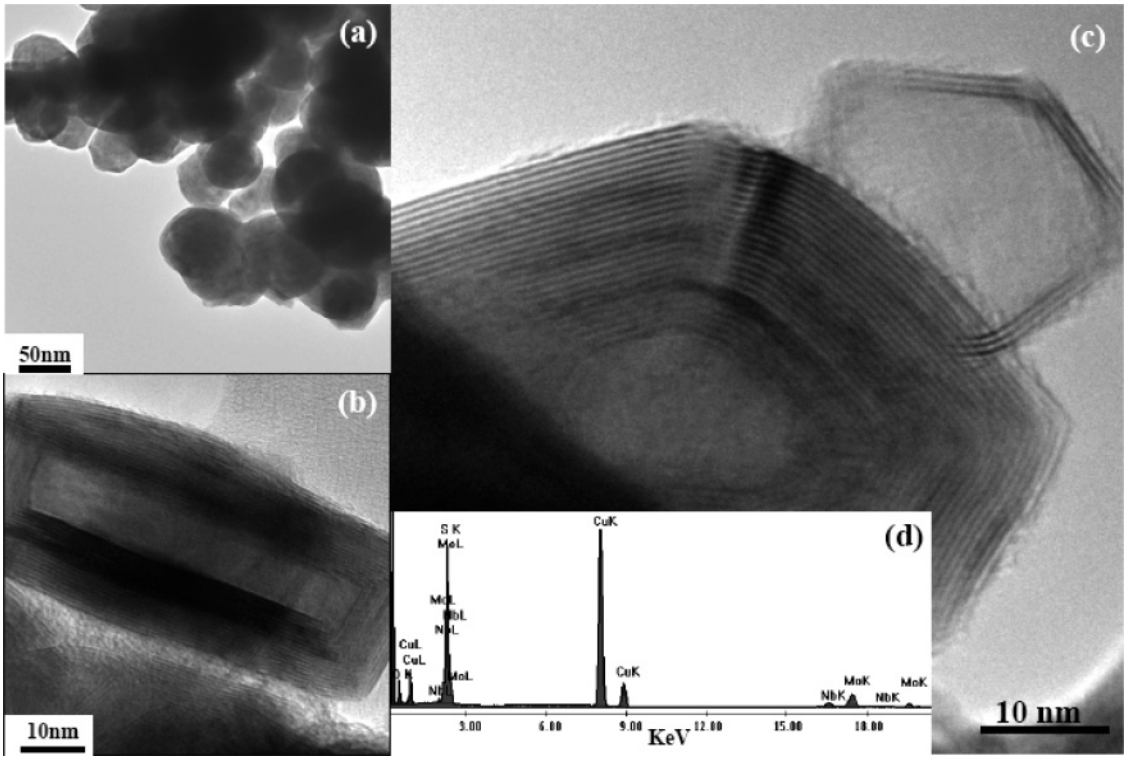

Figure 4. (a) TEM image of the IF-$Mo_{1-x}Nb_xS_2$ nanoparticles prepared at $T_1 = 800$ °C and $T_2 = 850$ °C (series 1), (b and c) HRTEM images of the IF-$Mo_{1-x}Nb_xS_2$ nanoparticles prepared at $T_1 = 850$ °C and $T_2 = 900$ °C (series 2). (d) EDS spectra of the IF-$Mo_{1-x}Nb_xS_2$ nanoparticle in (c).

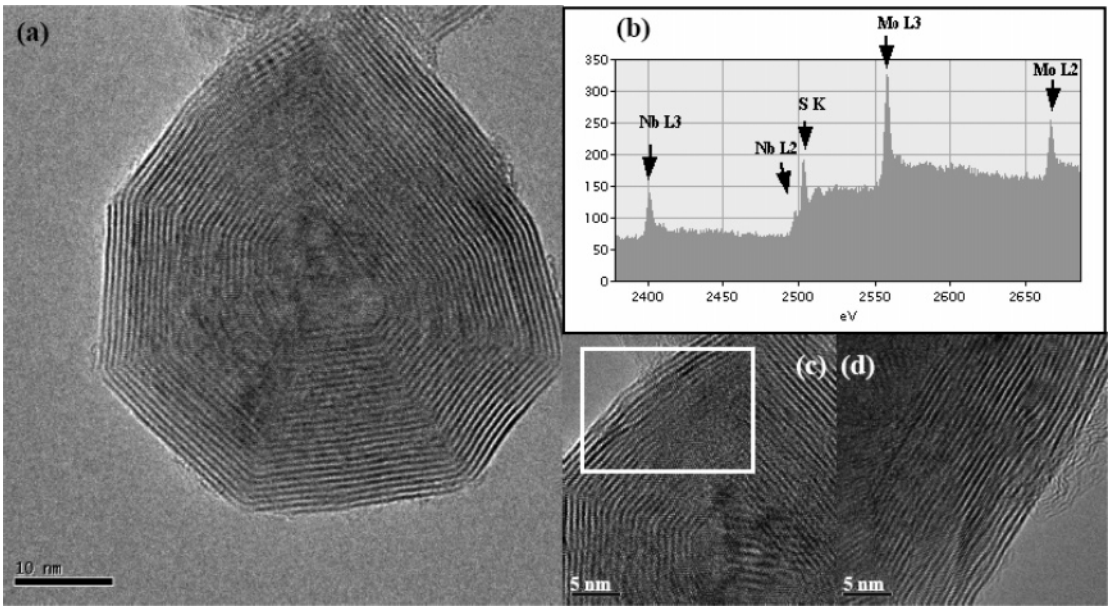

Figure 5. (a) HRTEM image and (b) the corresponding EELS spectrum of the IF-$Mo_{1-x}Nb_xS_2$ nanoparticles prepared at $T_1 = 850$ °C and $T_2 = 900$ °C (series 2). (c) Exploded view of a portion of nanoparticle in (a) showing mismatch in the layers. (d) HRTEM image of another IF nanoparticle showing defects/dislocations in the layers.

the Mo/Nb/S ratio remained nearly constant, independent of the IF nanoparticle diameter and position.

The low loss region in the EELS spectra shows two characteristic peaks: a plasmon peak at 23.3 ± 0.1 eV, which is shifted to lower energies by 0.2 eV relative to the pure IF-MoS_2 sample (23.5 ± 0.1 eV), and an additional feature at 8.2 $\pm$ 0.2 eV.[20a,b] However, this change is too small to be used to differentiate between the two modes of Nb insertion, either in the layers of the host lattice (MoS_2) or as an intercalating moiety in-between the MoS_2 layers. The very small shift in the plasmon energy is by itself important. One may expect a larger shift, however, in the same direction, under p-type doping of such very high levels. The fact that we see just a small shift is an indication though not a direct one. An enlarged view of a portion of a nanoparticle (shown in Figure 5a) shows a mismatch in the layers (Figure 5c). The HRTEM of another IF nanoparticle (Figure 5d) shows defects/dislocations in the layers.[10] The presence of the layers' mismatch, defects, and/or dislocations, in the case of the IF-$Mo_{1-x}Nb_xS_2$ nanoparticles, is another indication of the incorporation of Nb atoms in the lattice of

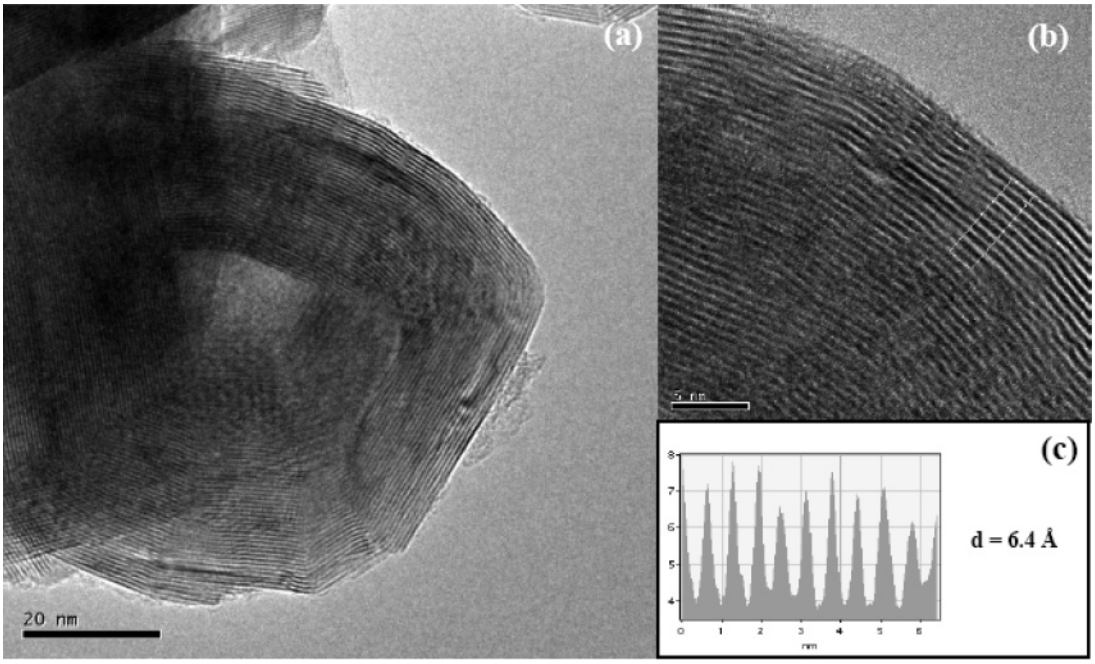

Figure 6. (a) HRTEM image and (b) the expanded view of a portion of the IF-$Mo_{1-x}Nb_xS_2$ nanoparticles prepared at $T_1 = 850$ °C and $T_2 = 900$ °C (series 2). (c) Line profile of the boxed area in (b) shows the interlayer spacing to be 6.4 Å.

MoS_2. The occurrence of such defects is not surprising considering the difference in coordination of the two metal atoms (trigonal biprism for the Mo and octahedral for the Nb atom). These kind of defects were very rare in the case of the pure IF-MoS_2 nanoparticles.[8a]

Figure 6a and 6b show the HRTEM image and the corresponding expanded view of a portion of the IF-$Mo_{1-x}Nb_xS_2$ nanoparticles prepared at $T_1 = 850$ °C and $T_2 = 900$ °C (series 2). The interlayer spacing is 6.40 Å as revealed by the line profile of the framed area in Figure 6c. Although this spacing is observed in some cases (see section on xrd), this does not seem to be the rule for all the IF-$Mo_{1-x}Nb_xS_2$ nanoparticles, since some of them exhibit the 6.20 Å spacing which is typical for the pure IF-MoS_2 nanoparticles. The observed expansion in the case of IF-$Mo_{1-x}Nb_xS_2$ nanoparticles seems to be too small to be attributed to intercalation of Nb in-between the layers. Previously, alkali metal intercalation of IF-MoS_2 and IF-WS_2 nanoparticles resulted in a lattice expansion of 2−3 Å.[9a] Furthermore, electron diffraction (ED) analysis of individual IF-$Mo_{1-x}Nb_xS_2$ nanoparticles does not support such an intercalation.[21a,b] The diffraction pattern did not reveal any additional spots that may arise due to Nb intercalation.

This is also in good agreement with the XRD diffraction data. As mentioned above NbS_2 may appear in two polytypes, hexagonal-2H (*P*63/*mmc*) and rhombohedral-3R (*R*3*m*). The present XRD data (see Figures 2 and 3) agree well with that of the 2H polytype. Thus in this case, defects and dislocations in the layers, arising due to the incorporation of Nb in the layers, seem to be responsible for the observed increase in the layer spacing. It must be taken into account the fact that intercalation of IF nanoparticles with, e.g., alkali metal atoms was found to be very nonuniform with internal layers of the IF nanoparticles unaffected at all. The fact that the Nb is distributed uniformly in the present IF-$Mo_{1-x}Nb_xS_2$ nanoparticles indicates that there is much less strain here as compared to the case of alkali metal intercalation in IF nanoparticles. Presumably lattice substitution of Nb into the MoS_2 network is much less energetically demanding than intercalation, which leads to a large expansion in the interlayer distance.

Elemental mapping by energy-filtered TEM (EFTEM) analysis revealed the presence of Nb uniformly throughout the particles. Apart from the uniform Nb substitution into the MoS_2 lattice, there is also a very thin amorphous niobium oxide layer seen as an outer envelope on the IF nanoparticles (Figure 7).[12d] The stoichiometry of niobium oxide and the oxidation of niobium metal are of considerable interest, especially in the realm of superconductivity. Niobium oxide is known to exist in three principal forms: Nb_2O_5, NbO_2, and NbO, but several suboxides of the form NbO_x ($x < 1$) are also known, and the structure of many of these have been reported.[22a,b] In the present case however since the nature of the oxide is amorphous, it was not possible to ascertain the exact phase of the niobium oxide layer sheathing the IF-$Mo_{1-x}Nb_xS_2$ nanoparticles. A summary of all the data is presented in Table 2 comparing the 2H-MoS_2 (2H-NbS_2), IF-MoS_2 (IF-NbS_2), and the IF-Mo_{1-x}-Nb_xS_2 nanoparticles.

3.3. X-ray Photoelectron Spectroscopy (XPS). Table 3 summarizes the XPS data of the IF-$Mo_{1-x}Nb_xS_2$ nanoparticles (series 2) given as the atomic concentration of the different elements. Figure 8 shows the corresponding Nb 3d spectrum, showing three doublets. The two low-energy doublets correspond to a reduced Nb moiety, presumably within the dichalcogenide layers, while the high-energy doublet is associ-

(20) (a) Enyashin, A. N.; Gemming, S.; Bar-Sadan, M.; Popovitz-Biro, R.; Hong, S. Y.; Prior, Y.; Tenne, R.; Seifert, G. *Angew. Chem., Int. Ed.* **2007**, *46*, 623. (b) Bar-Sadan, M.; Enyashin, A. N.; Gemming, S.; Popovitz-Biro, R.; Hong, S. Y.; Prior, Y.; Tenne, R.; Seifert, G. *J. Phys. Chem. B* **2006**, *110*, 25399.

(21) (a) Remskar, M.; Skraba, Z. *Surf. Sci.* **1996**, *365*, L652. (b) Zhou, C.; Hobbs, L. W. *Mater. Res. Soc. Symp. Proc.* **1993**, *295*, 195.

(22) (a) Terao, W. *Jpn. J. Appl. Phys.* **1963**, *2*, 156. (b) Magnumen, N.; Quinones, L.; Dufner, D .C.; Cocke, D. L.; Schweikert, E. A. *Chem. Mater.* **1989**, *1*, 220.

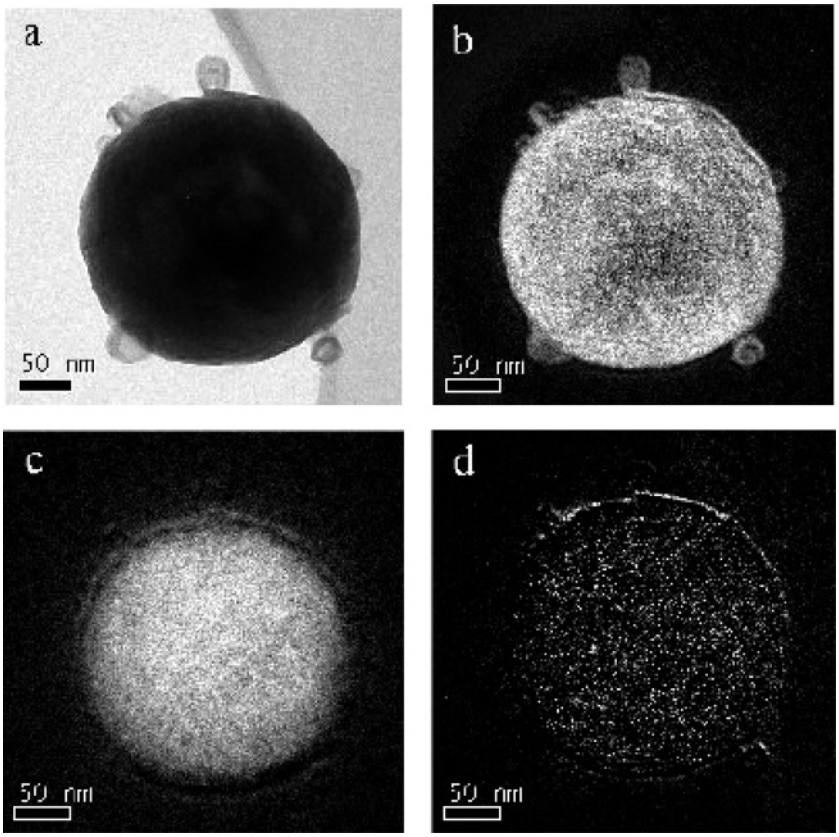

Figure 7. Images of elemental mapping by energy-filtered TEM (EFTEM) of IF-$Mo_{1-x}Nb_xS_2$ nanoparticle, with a surface oxide layer. (a) Zero-loss image. (b) Sulfur map measured around the S $L_{2,3}$ edge (167−187 eV). (c) Niobium map measured around the Nb L_3 edge (2370−2470 eV). (d) Oxygen map measured around the O K edge (532−562 eV).

Table 2. Comparison of the 2H-MoS_2, 2H-NbS_2, IF-MoS_2, IF-NbS_2 with IF-$Mo_{1-x}Nb_xS_2$ (Obtained in the Present Study)

			additional information	
	polytypes	size	composition	type
MoS_2	hexagonal-2H (*P*63/*mmc*) $c/2 = 6.15$ Å rhombohedral-3R = 6.06 Å	−	−	−
NbS_2	hexagonal-2H (*P*63/*mmc*) $c/2 = 5.981$ Å rhombohedral-3R (*R*3*m*) = 5.96 Å	−	−	−
IF-MoS_2[8a]	hexagonal-2H (*P*63/*mmc*) $c/2 = 6.20$ Å	∼50 nm	Mo/S 1:2	spherical/faceted nanoparticles
IF-NbS_2[12d]	rhombohedral-3R (*R*3*m*) $c/2 = 6.15$ to 5.9 Å depending on annealing	20−40 nm (small particles) 60−80 nm large particles)	Nb/S 1:2	spherical nanoparticles
IF-$Mo_{1-x}Nb_xS_2$	hexagonal-2H (*P*63/*mmc*) $c/2 = 6.40$ Å	∼40−50 nm (90% small particles) ∼200 nm (large particles 10%)	15−25% Nb NbO_x surface layer	spherical/faceted nanoparticles

ated with oxidized (external) Nb (as also revealed by energy filtered TEM).

The binding energies of Mo and S exhibit a marked difference when the Nb-substituted and the unsubstituted samples are compared: Mo($3d_{5/2}$) at 228.9 and 229.3, respectively, and S($2p_{3/2}$) at 161.7 and 162.1, respectively. This is clear evidence for incorporation of Nb into the Mo-based particles. The observed difference, which is practically identical for the Mo and S lines, 400 ± 100 meV, is far beyond any possible charging effect (see CREM data below). Also, it does not show up at the gold and carbon signals (and has a different magnitude for the oxygen). These findings indicate that this binding energy difference is associated with a Fermi level shift. Thus, the Fermi level of the Nb-substituted nanoparticles (IF-$Mo_{1-x}Nb_xS_2$) is shifted toward lower energies, making them more "p-type".

A unique way to test the electrical properties of the nanoparticles is provided by a new technique baptized as chemically resolved electrical measurements (CREM),[15,23−25] which is a "top-contact-free" electrical characterization method. This technique allows for the determination of the electrical response of

(23) Cohen, H.; Nogues, C.; Zon, I.; Lubomirsky, I. *J. Appl. Phys.* **2005**, *97*, 113701.
(24) Cohen, H.; Sarkar, S. K.; Hodes, G. *J. Phys. Chem. B* **2006**, *110*, 25508.
(25) Cohen, H.; Maoz, R.; Sagiv, J. *Nano Lett.* **2006**, *6*, 2462.

Table 3. Extraction of Surface Composition from Net Area (Numerical Integration of Area under the Peak)

element	atomic concn (%)
Nb^{red}	0.37
Nb^{ox}	1.15
Mo	3.31
S	7.77
S^{ox}	0.78
O	3.15
C	30.6
Au	24.81

the different nanoparticles. By measuring the current flow to the ground and monitoring the energy shift of a given element in the surface layer during electron bombardment by the flood gun, the internal potential drop in the layer which contains this specific element can be determined. Figure 9 shows XPS line shifts of series 2 IF-$Mo_{1-x}Nb_xS_2$ nanoparticles under a given electrical input signal (eFG filament current of 1.75 A). The line shifts reflect the local potential changes at addresses associated with the inspected chemical element. This experiment is conducted with the nanoparticles deposited on a gold substrate, and complementary CREM data (not shown) are recorded also for the gold, carbon, and oxygen signals. All gold substrates exhibited a small electron-beam induced shift of the XPS signal, signifying a relatively good Ohmic back contact.

The film of the IF-MoS_2 nanoparticles exhibits measurable line shifts upon electron irradiation with the eFG (see the Mo line in Figure 9c). This line shift directly reflects a local potential change, presumably due to the internal resistance of the nanoparticle (under the incident electron flux). The internal resistance of the nanoparticle is estimated to be on the order of a few hundred kiloohms. In contrast, the Mo line of the IF-$Mo_{1-x}Nb_xS_2$ nanoparticles does not show any observable line shift (see Figure 9b), indicating that the nanoparticle resistance is low, such that only small, undetectable potential changes can evolve under the applied electrical signal (the input eFG current). Interestingly, the Nb line itself consists of two electrically different components (see Figure 9a). As mentioned above, the low binding energy components (203.70 and 204.80 eV) are attributed to atoms incorporated within the Mo-based particles, and they do not shift under the input flux of the electrons. The other component (at 208.40 eV), which is associated with external oxidized Nb species, does exhibit a strong line shift under the electron flux (Figure 9a). This shift is similar in magnitude to that of the oxygen line (not shown). Based on complementary data (EFTEM, see above), the oxidized Nb appears to comprise a sub-nanometer coating on the nanoparticle surface. This means that contact electrical measurements (e.g., with AFM, see below) may be subjected to an oxide barrier, which is not the case for the noncontact CREM approach.

Finally, the CREM results are in good agreement with the observation of an XPS-derived Fermi level shift upon Nb substitution, which is manifested through the shift of the Mo and S lines to lower energies in the Nb substituted (alloyed) IF nanoparticles. The incorporation of Nb into the semiconducting IF-MoS_2 nanoparticles induces enhanced p-type behavior, where the Fermi level shifts down toward the valence band, and the electrical conductance increases accordingly.

3.4. Conducting Atomic Force Microscopy (c-AFM). Figure 10a shows a representative AFM image of an individual

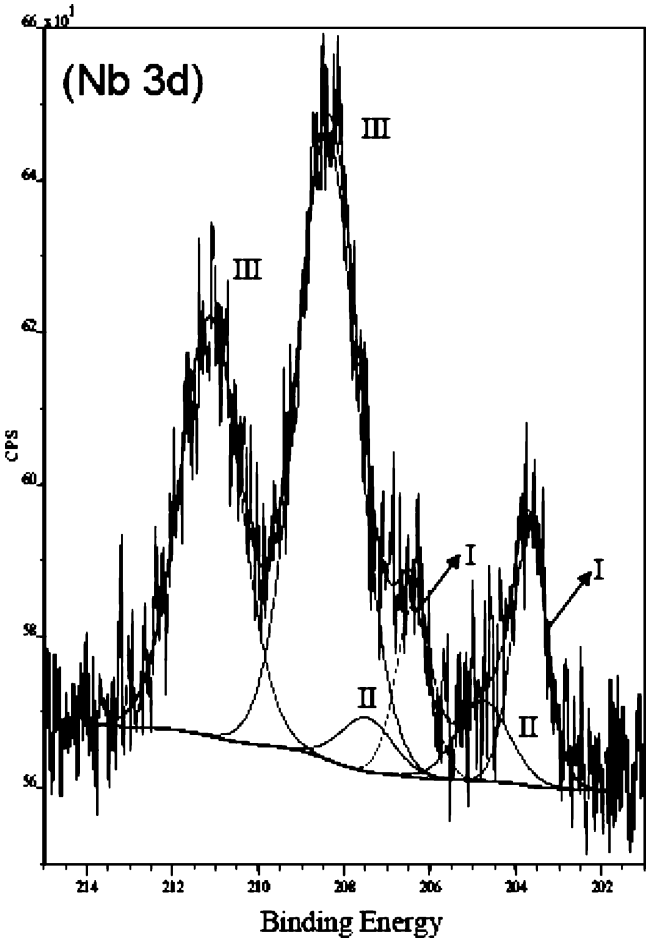

Figure 8. Line shape analysis of the Nb 3d signal (with Gaussian−Lorenzian components). Reduced Nb (I and II) is believed to be within the nanoparticles. The oxidized Nb (III) appears on particle surfaces.

IF-$Mo_{1-x}Nb_xS_2$ nanoparticle (series 2). AFM measurements were also carried out on IF-MoS_2 nanoparticles for comparison.[26−29] Typical *I*/*V* curves of the IF-$Mo_{1-x}Nb_xS_2$ and IF-MoS_2 nanoparticles are shown in Figure 10b. Whereas the IF-MoS_2 nanoparticle exhibits a noticeable band gap region where no current flows,[26−29] the IF-$Mo_{1-x}Nb_xS_2$ nanoparticles exhibit only an inflection in the curve where current is reduced, but not to zero. Furthermore, the current rise is significantly sharper for the IF-$Mo_{1-x}Nb_xS_2$ nanoparticles. Calculated d*I*/d*V* vs *V* traces of the curves in Figure 10b are shown in Figure 10c. From these curves, the effective band gap was measured. In both cases, the distribution is quite broad, representing both variations between the different particles and experimental fluctuations. An average band gap of ∼1.05 eV (±0.2 eV) was estimated for a canonical ensemble of the IF-MoS_2 nanoparticles. This result strongly suggests that the IF-MoS_2 nanoparticles are semiconductors. The band gap of the bulk 2H-MoS_2 phase is l.2 eV.[26−29] The somewhat smaller gap of the nanoparticles, compared with the values of the bulk phase, may be attributed to the expansion of *c*/2 (vdW gap) in various regions of the

(26) (a) Kam, K. K.; Parkinson, B. A. *J. Phys. Chem.* **1982**, *86*, 463. (b) Parkinson, B. A.: Furtak, T. E.; Canlicld, D.; Kam, K.; Kline, G. *Faraday Discuss. R. Soc. Chem.* **1980**, *70*, 1.
(27) Hershfinkel, M.; Gheber, L. A.; Volterra, V.; Hutchison, J. L.; Margulis, L.; Tenne, R. *J. Am. Chem. Soc.* **1994**, *116*, 1914.
(28) Homyonfer, M.; Alperson, B.; Rosenberg, Y.; Sapir, L.; Cohen, S. R.; Hodes, G.; Tenne, R. *J. Am. Chem. Soc.* **1997**, *119*, 2693.
(29) Frey, G. L.; Elani, S.; Homyonfer, M.; Feldman, Y.; Tenne, R. *Phys. Rev. B* **1998**, *57*, 6666.

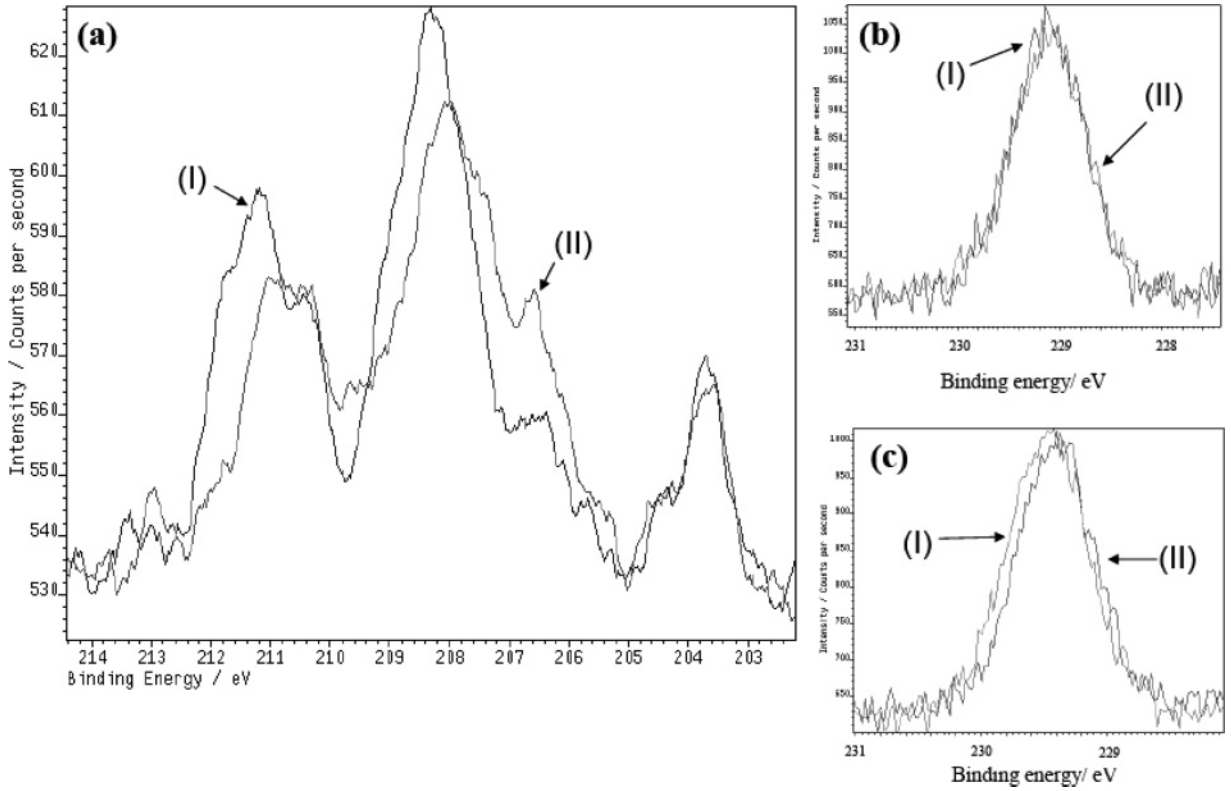

Figure 9. (a) Electrically induced line shifts of (a) Nb(3d), (b) Mo ($3d_{5/2}$) in IF-$Mo_{1-x}Nb_xS_2$ nanoparticles, and (c) Mo ($3d_{5/2}$) in IF-MoS_2 nanoparticles. In all panels, curve (I) corresponds to "eFG off" conditions and curve (II) refers to "eFG on". Note that (panel a) the oxidized Nb exhibits a large shift while the reduced Nb signal is practically not shifted at all. Comparison of panels (b) and (c) demonstrates the effect of Nb substitution on the Mo line shift, indicating improved conductance in the IF-$Mo_{1-x}Nb_xS_2$ nanoparticles.

nanoparticles, due to the strain involved in the folding of the structure. An alternative explanation for the reduced gap of the nanoparticles is that sub-band gap states, which emanate from structural imperfections or edge dislocations, may serve as mediators for tunneling of charge and hence increase the current under bias.[26b] In contrast to the IF-MoS_2 nanoparticles, the IF-$Mo_{1-x}Nb_xS_2$ exhibits a metallic character. A minority of the particles measured (15%) showed an apparent gap of up to 0.6 eV which indicates the presence of an additional barrier in the tunneling gap. This is likely provided by the sheathed amorphous niobium oxide layer observed in the TEM measurements. It is possible that this layer is disrupted and penetrated by the tip in most measurements.

The experimental *I*/*V* curves can be further analyzed to derive the effective resistance. The values were determined over a 0.3 V bias range starting directly after the current rises above the noise level. After accounting for the intrinsic point contact resistance of the tip as measured on the clean Au surfaces, the IF-$Mo_{1-x}Nb_xS_2$ nanoparticles have a resistance of 10 megaohm, as opposed to 60 megaohm for the undoped IF-MoS_2. Considering the existence of an oxide layer in some of the particles examined by TEM, part of this resistance is likely mediated by the quality of the contact.

3.5. Scanning Tunneling Microscopy and Spectroscopy (STM and STS). To further decipher the electronic properties of IF-$Mo_{1-x}Nb_xS_2$ nanoparticles (series 2) STM/STS measurements were carried out at room temperature and at 4.2 K. In Figure 11, a typical tunneling spectrum acquired at room temperature on such particles is presented, in comparison with a representative measurement performed on IF-MoS_2 nanoparticles. Consistent with the c-AFM measurements described above, the room-temperature STS data reveal vastly different behaviors for these two types of particles. The spectra taken on the IF-MoS_2 nanoparticles as depicted in Figure 11a manifest typical semiconductor-like features. They exhibited pronounced gaps (namely, regions around zero bias where the current is below the noise level) ranging between 0.9 and 1.4 eV. It should be noted here that these values do not necessarily correspond to the actual gaps, since the apparent (measured) gaps may be broadened due to a voltage division between the two tunneling junctions: tip−particle and particle−substrate.[16] Nevertheless, a clear gap around zero bias was always observed. In contrast, no gaps were detected on the IF-$Mo_{1-x}Nb_xS_2$ nanoparticles, and the spectra exhibited Ohmic behavior around zero bias (Figure 11b). For comparison, a typical spectrum measured on the bare gold substrate is shown (Figure 11c). Note that the typical currents measured on the IF-$Mo_{1-x}Nb_xS_2$ particles were significantly smaller than those measured on the Au substrate, and they also revealed a subtle additional structure. This behavior may reflect the DOS of the IF-$Mo_{1-x}Nb_xS_2$ nanoparticles around the Fermi energy, which, according to recent DFTB calculations (see below), is not constant over the corresponding voltage range.

A more complex behavior—single electron tunneling (SET) characteristics,[16] namely, the Coulomb blockade and Coulomb staircase—was found with the IF-$Mo_{1-x}Nb_xS_2$ nanoparticles (series 2) at 4.2 K, as depicted by Figure 12. The *I*/*V* curves in parts a and b, and the corresponding d*I*/d*V* vs *V* spectra (solid lines in Figure 12c and 12d, respectively), were acquired with slightly different STM settings. This is known to affect the offset

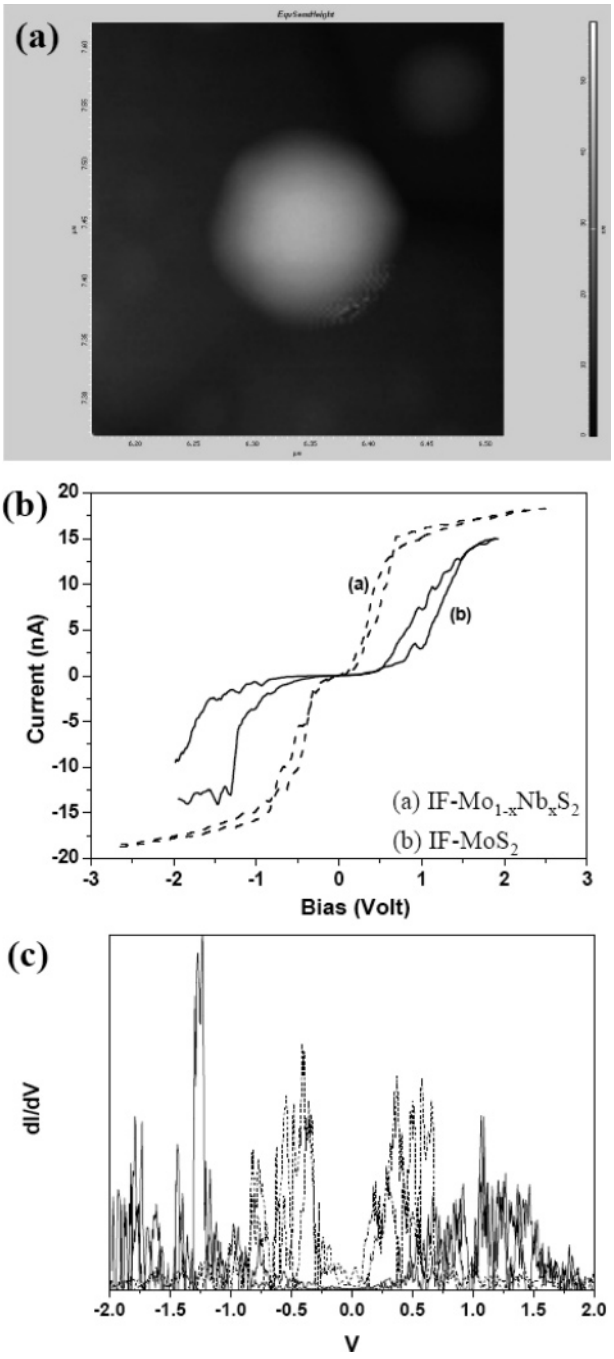

Figure 10. AFM measurements carried out on an IF-$Mo_{1-x}Nb_xS_2$ nanoparticle (a) AFM image, (b) *I*/*V* curves carried out on the nanoparticle (dashed lines), (c) corresponding d*I*/d*V* vs *V* plots. In both (b) and (c), the corresponding plots of the IF-MoS_2 nanoparticle are shown for comparison (solid lines).

potential or "residual charge", Q_0, and consequently the tunneling conductance around zero bias (in the Coulomb blockade regime).[16,30] This effect is evident by comparing Figure 12c and 12d. These spectra could be quite well reproduced using simulations based on the "orthodox model" for SET through a metallic particle in a double barrier tunnel junction configuration.[16,30] The simulation results are presented by the dashed curves in Figure 12 (c and d). The good agreement between the measured and simulated peak position indicates that these

(30) Bar-Sadeh, E.; Goldstein, Y.; Zhang, C.; Deng, H.; Abeles, B.; Millo, O. *Phys. Rev. B* **1994**, *50*, R8961.

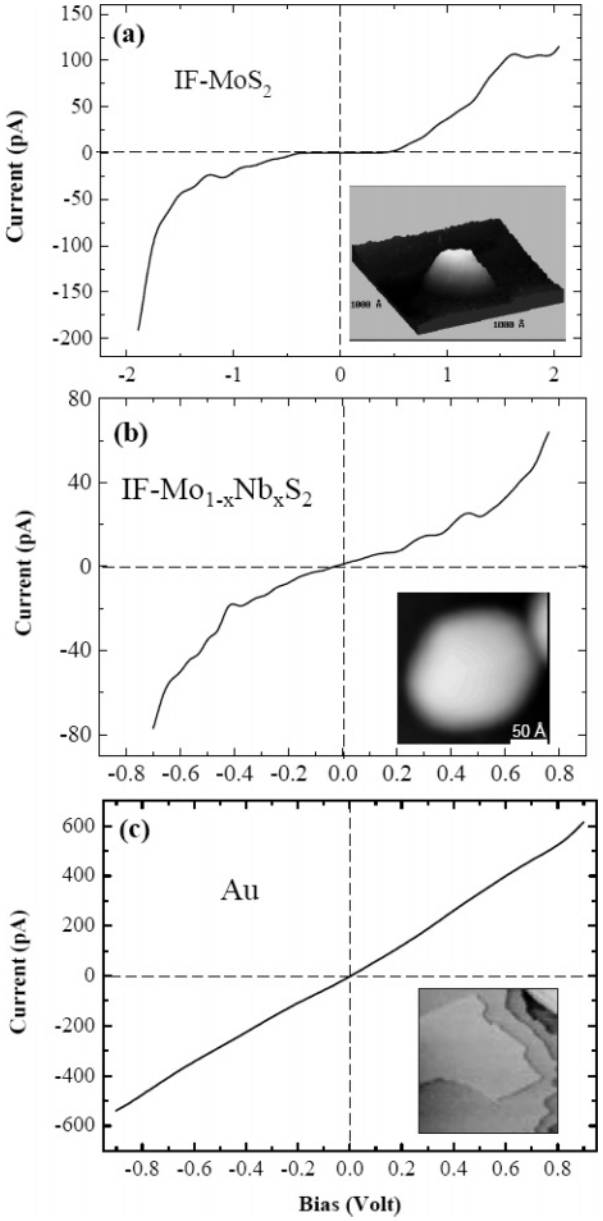

Figure 11. *I*/*V* curves at room temperature measured on (a) an IF-MoS_2 nanoparticle (~40 nm diameter), (b) an IF-$Mo_{1-x}Nb_xS_2$ nanoparticle (~30 nm diameter), and (c) the gold substrate. The insets show the corresponding topographic images. The image in (c) is 1×1 mm^2 in size, revealing atomic steps on the Au(111) surface.

particles are metallic-like, revealing no signature of discrete states or semiconductor gap. Moreover, the observed charging energies of about 50 meV are also consistent with metallic particles of a size similar to that of the IF nanoparticles. A best fit to spectrum c was obtained with capacitance and resistance values of $C_1 = 1.1$ aF and $R_1 = 100$ MΩ for the substrate−particle junction, $C_2 = 2.6$ aF and $R_2 = 260$ MΩ for the tip−particle junction, and $Q_0 = 0.03e$ (e being the electron charge). The values corresponding to spectrum d are $C_1 = 1.1$ aF, $R_1 = 100$ MΩ, $C_2 = 2.2$ aF, $R_2 = 420$ MΩ, and $Q_0 = -0.4e$.

4. Discussion

4.1. Modification of the Electronic Properties. The effect of Mo → Nb substitution on the electronic structure of MoS_2 nanotubes has been investigated using the density functional tight binding method (DFTB).[11] It is of interest to compare these

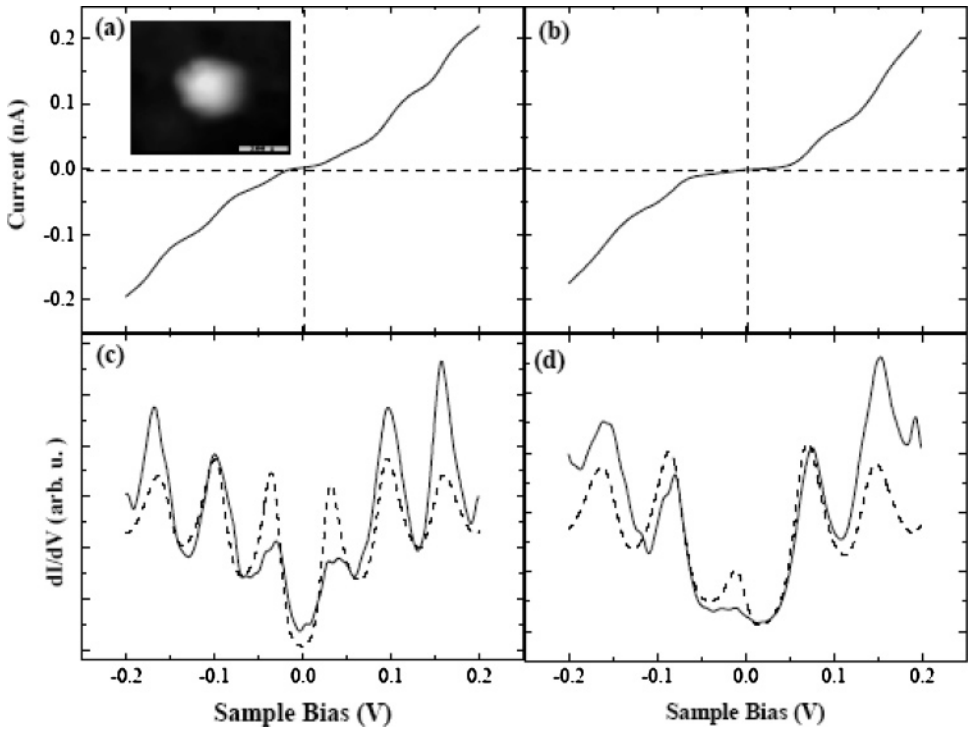

Figure 12. Tunneling spectra acquired at 4.2K on the IF-$Mo_{1-x}Nb_xS_2$ nanoparticle (~30 nm diameter) shown in the inset, exhibiting pronounced SET effects. The *I*/*V* curves in (a) and (b) were measured with slightly different settings (see text). The corresponding d*I*/d*V* vs *V* curves are shown in (c) and (d), respectively (solid lines). The dashed are fits to the "orthodox model" for SET in a double barrier tunnel junction configuration.

calculations with the c-AFM and STS results reported above, although the IF-$Mo_{1-x}Nb_xS_2$ nanoparticles are expected to differ from the analogous nanotubes in a number of ways. The Mo → Nb substitution leads to the formation of new states in the band gap of MoS_2 nanotubes. With increasing Nb content (i.e., with a decreasing number of electrons in comparison with "pure" MoS_2), the Fermi level is shifted and correspondingly the density of states (DOS) near the Fermi energy is increased, consistent with the XPS and CREM data. As a consequence, the DOS close to the Fermi level of Nb-substituted MoS_2 can be tuned over a wide range, by the degree of substitution. Also the IF-$Mo_{1-x}Nb_xS_2$ nanoparticles exhibit metallic character, independent of the substitution patterns of the Nb atoms. Currently, the control over the extent of Nb substitution of the IF nanoparticles is rather limited. However, the observed changes in the electronic characteristics as exemplified by apparently a reduced band gap and resistance are in qualitative agreement with the first-principles predictions of the respective nanotubes. To allow for a more quantitative comparison, a more systematic approach, whereby, e.g., the size of the nanoparticles and their Nb content will be varied and the changes in the electronic transport properties of the nanoparticles determined, is necessary.

4.2. Substitutional Pattern of the Nb Atoms within the IF-$Mo_{1-x}Nb_xS_2$ Lattice. The analysis of the various data presented above leads to the following points. From the X-ray diffraction data it is possible to conclude that the as-synthesized IF-$Mo_{1-x}Nb_xS_2$ nanoparticles is comprised of two phases corresponding to those of (Nb doped) MoS_2 and NbS_2. The presence of a distinct phase with Nb as an intercalant is supported by neither the XRD nor the electron diffraction. If it existed, such a phase would be revealed by typical (00*l*) peaks at lower angles (larger interlayer spacing).[9a] The presence of a broad (002) peak (and the shift of this peak toward the position of (002) reflection of NbS_2) suggests the existence of fragments of a NbS_2 lattice incorporated turbostratically among the MoS_2 layers. Furthermore the presence of only (*hk*0) peaks of NbS_2 suggests the presence of the respective single layers. However according to Vegard's law,[31] a small shift in the positions of the (110) peak in the case of the IF-$Mo_{1-x}Nb_xS_2$ nanoparticles toward the position of (110) reflection of NbS_2 may denote that substitution of a minor part (about 3%) of individual Mo atoms by individual Nb atoms into the MoS_2 structure is likely (in addition to the NbS_2 nanosheets interspersed in the MoS_2 structure). It is necessary to point out that the corresponding change of the lattice parameter is so small that an expected shift of another in-plane (100) peak at 32.7° will be comparable with the error of the measurement and consequently cannot be observed. Thus in addition to the sheets/stripes of NbS_2 present turbostratically among the MoS_2 layers, there is also the replacement of Mo atoms individually by Nb atoms in the case of the IF-$Mo_{1-x}Nb_xS_2$ nanoparticles.

TEM analysis reveals the presence of well faceted nanoparticles of diameter 40−50 nm. EDS and EELS measurements show the presence of Mo, Nb, S on the same individual nanoparticles, with Nb uniformly distributed over the entire nanoparticle. The concentration of Nb in each of the individual nanoparticles present is ascertained to be around ~15−25% by TEM-EDS and HRTEM-EELS analysis. In some IF nanoparticles the interlayer spacing increases to 6.4 Å possibly due to defects and/or dislocations within the layer arising as a result of Nb incorporation, while in others the interlayer spacing remains at 6.2 Å (note that Nb is present uniformly in these IF nanoparticles as well). HRTEM-EELS chemical mapping reveals the presence of Nb distributed uniformly throughout the

(31) (a) Agarwal, M. K.; Wani P. A. *Mater. Res. Bull.* **1979**, *14*, 825. (b) Denton, A. R.; Ashcroft, N. W. *Phys. Rev. A* **1991**, *43*, 3161.

Scheme 1. Substitutional Pattern of the Nb Atoms within the IF−$Mo_{1-x}Nb_xS_2$ Lattice

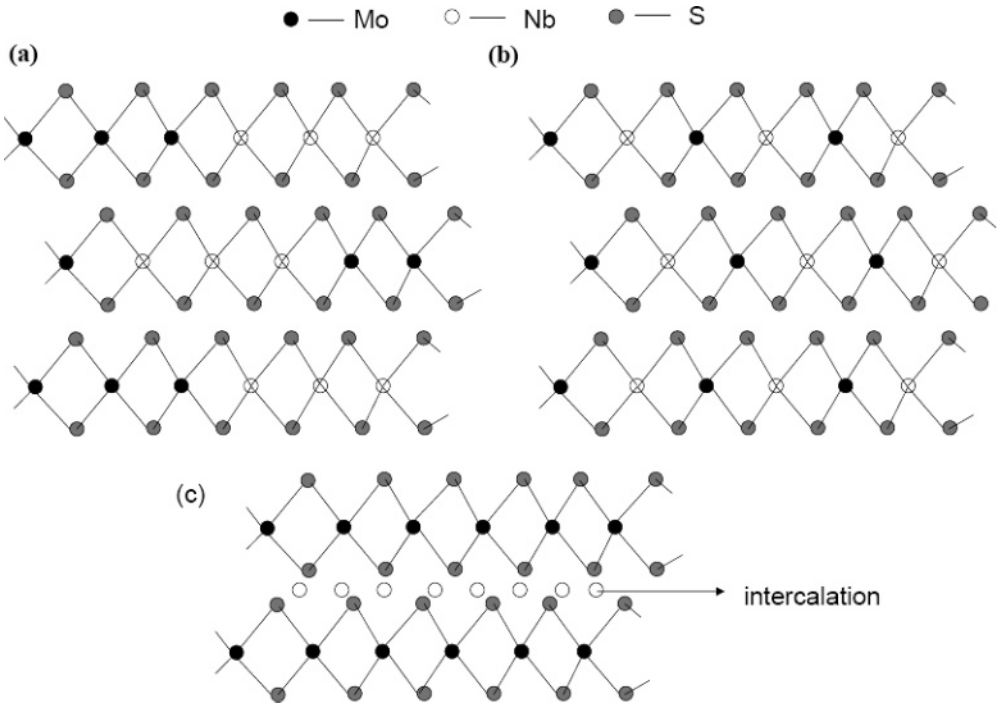

nanoparticles. It must be taken into account that intercalation of alkali metal atoms in the van der Waals gap of the IF nanoparticles was found to be very nonuniform with internal layers of the IF nanoparticles unaffected at all.[9a] The fact that the Nb is distributed evenly in the individual IF-$Mo_{1-x}Nb_xS_2$ nanoparticle and the absence of any local variations in the chemical composition excludes Nb intercalation as a potential major mechanism for altering the IF-MoS_2 lattice. Thus the Nb seems to be incorporated within the MoS_2 layers. In addition from the EFTEM observations the presence of an oxide layer covering the nanoparticles is observed.

The XPS shows two low binding-energy doublets corresponding to reduced Nb moieties, presumably within the dichalcogenide layers, and a high-energy doublet associated with oxidized Nb, which is likely to be present on the surface (from complementary analysis, as also revealed by energy filtered TEM). One of these reduced species is believed to correspond to the sheets of NbS_2, while the other one probably corresponds to alternate substitutional sites of individual Nb atoms at Mo atomic sites.

A schematic of three possible types of Nb incorporation within the lattice of MoS_2 is presented in Scheme 1. Scheme 1a represents the case where there are continuous spreads of both types of atoms within each layer alternating randomly turbostratically in Scheme 1b. Mo and Nb atoms are alternately incorporated into the lattice of MoS_2, whereas Scheme 1c shows the unlikely case of intercalation of atoms in the van der Waals gap between the layers. The Nb incorporation could be a combination of the first two types.

The two kinds of Nb species could have a different effect on the electronic properties of the IF-$Mo_{1-x}Nb_xS_2$ nanoparticles. Individual Nb atoms in substitutional sites could play the role of a dopant, leading to a downward shift of the Fermi level closer to the valence band and increased conductivity. Patches of NbS_2 sheets interspersed in the MoS_2 lattice are likely to impose a metallic character on the nanoparticle. The apparent "soft gap", manifested by the reduced (but not totally suppressed) current around zero bias, as measured by conductive AFM could be also influenced by the size of the nanoparticles, with the larger nanoparticles exhibiting a larger gap.[32,33] It should be noted that there is some quantitative disagreement between the c-AFM and the STM data, in the degree of current suppression around zero bias in the spectra of the IF-$Mo_{1-x}Nb_xS_2$ nanoparticles, the latter hardly revealing the "soft gap". This disagreement is almost semantic, since both tips suffer from a contact potential difference with the nanoparticle itself, making an absolute determination of the band gap somewhat uncertain. In addition, the Nb-oxide layer at the IF particle shell does not affect much the contactless STS measurements (in contrast to the case of c-AFM, discussed above), since its contribution to the tunneling resistance is probably smaller than that of the vacuum tunnel barrier. However, the present measurements leave no doubt that the Nb incorporation into the 2H-MoS_2 lattice of the IF reduces the resistivity of the nanoparticle substantially. In order to study these effects more quantitatively a series of samples with different Nb content should be prepared, which is reserved for a future work.

5. Conclusions

IF-$Mo_{1-x}Nb_xS_2$ nanoparticles have been prepared starting from the respective chloride vapor precursors in addition with H_2S. The IF-$Mo_{1-x}Nb_xS_2$ nanoparticles have been extensively characterized by XRD, TEM-EDS, HRTEM-EELS, and XPS. From the detailed investigation of the electrical properties by STM and AFM analysis, the substitution of Nb for Mo involves a semiconductor to metallic type transformation (IF-MoS_2 are known to be semiconductors). This is in accordance with the calculations of Seifert et al.[11] who have shown that the IF-Mo_{1-x}-

(32) Scheffer, L.; Rosentzveig, R.; Margolin, A.; Popovitz-Biro, R.; Seifert, G.; Cohen, S. R.; Tenne, R. *Phys. Chem. Chem. Phys.* **2002**, *4*, 2095.
(33) Seifert, G.; Terrones, H.; Terrones, M.; Jungnickel, G.; Frauenheim, T. *Phys. Rev. Lett.* **2000**, *85*, 146.

Nb_xS_2 nanoparticles have metallic properties, independent of the substitution patterns of the Nb atoms. The IF-$Mo_{1-x}Nb_xS_2$ nanoparticles also show single electron tunneling (SET) characteristics. This study is an example of heteroatom substitution in the case of IF nanoparticles opening up a wide range of possibilities including varying the electronic behavior of the IF nanoparticles, in superconductivity and in spintronics.

Acknowledgment. R.T. is grateful to the Helen and Martin Kimmel Center for Nanoscale Science. He holds the professorial Drake Family Chair for Nanotechnology. We wish to thank also the Harold Perlman Foundation. O.M. and D.A. thank the Israel Science Foundation, Centers of Excellence program, and the European Union SA-NANO project for support. O.M. holds the Harry de Jur Chair for Applied Science.

Supporting Information Available: S1: TEM image of the IF-$Mo_{1-x}Nb_xS_2$ nanoparticles (overview) prepared at $T_1 =$ 850 °C and $T_2 =$ 900 °C (series 2). S2: HRTEM image of the IF-$Mo_{1-x}Nb_xS_2$ nanoparticle showing the amorphous NbO_x layer (shown by an arrow). This material is available free of charge via the Internet at http://pubs.acs.org.

JA074081B